iScience

Article

TP53 upregulation via aurora kinase inhibition overcomes primary failure to venetoclax in *BCL2*-rearranged lymphomas

Graphical abstract

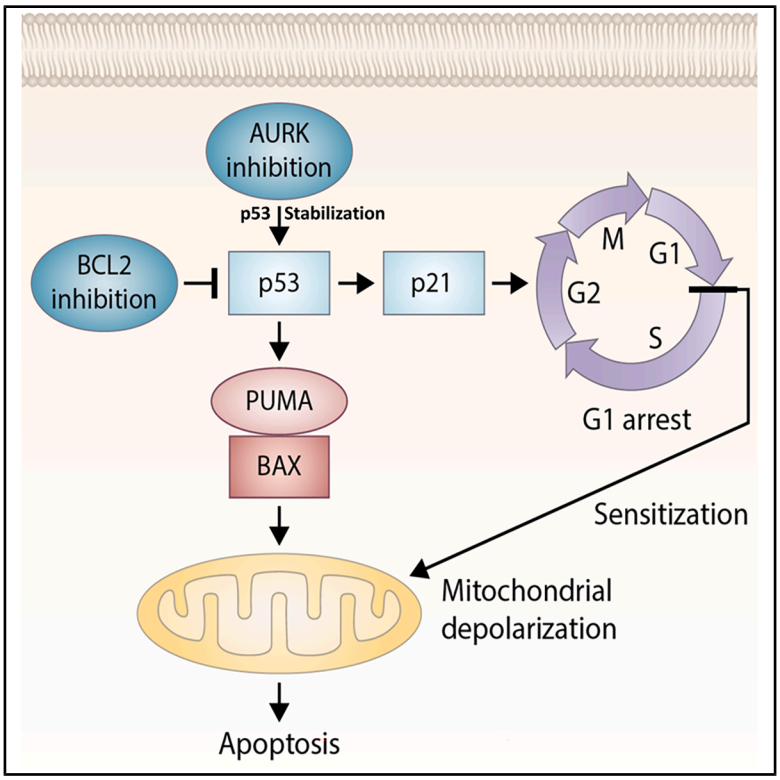

Authors

Rajeswaran Mani, Samon Benrashid, Margaret D. Templeton, ..., Donald L. Durden, Belinda R. Avalos, Steven I. Park

Correspondence

stepark@wakehealth.edu

In brief

Therapeutics; Molecular biology; Cancer

Highlights

- Bcl2 inhibition leads to p53/p21/Bax axis repression in *BCL2*-rearranged lymphoma
- Aurora kinase (Aurk) inhibition restores the p53/p21/Bax proapoptotic axis
- Inhibition of Bcl2 and Aurk is synthetically lethal in *BCL2*-rearranged lymphomas

Mani et al., 2025, iScience *28*, 112584
June 20, 2025
https://doi.org/10.1016/j.isci.2025.112584

CellPress

iScience

CellPress
OPEN ACCESS

Article

TP53 upregulation via aurora kinase inhibition overcomes primary failure to venetoclax in *BCL2*-rearranged lymphomas

Rajeswaran Mani,[1,8] Samon Benrashid,[1,8] Margaret D. Templeton,[1] Lawrence J. Druhan,[1,2] Sara L. Seegers,[1] Supriya Chakraborty,[1] Sarah E. Teague,[1] Scott C. Jaros,[1] Hsih-Te Yang,[3] David M. Foureau,[4] Nury M. Steuerwald,[5] Dhananjaya Pal,[6] Nilanjan Ghosh,[1,7] Edward A. Copelan,[1,7] Donald L. Durden,[6,7] Belinda R. Avalos,[1,7] and Steven I. Park[1,7,9,*]

[1]Department of Hematologic Oncology and Blood Disorders, Atrium Health Levine Cancer Institute, Charlotte, NC 28204, USA
[2]Department of Cancer Biology, Wake Forest University School of Medicine, Winston-Salem, NC 27101, USA
[3]Center for Cancer Biostatistics, Atrium Health Levine Cancer Institute, Charlotte, NC 28204, USA
[4]Immune Monitoring Laboratory, Atrium Health Levine Cancer Institute, Charlotte, NC 28204, USA
[5]Molecular Biology and Genomics Laboratory, Atrium Health Levine Cancer Institute, Charlotte, NC 28204, USA
[6]Molecular Targeted Therapeutics, Atrium Health Levine Cancer Institute, Charlotte, NC 28204, USA
[7]Department of Internal Medicine, Wake Forest University School of Medicine, Winston-Salem, NC 27101, USA
[8]These authors contributed equally
[9]Lead contact
*Correspondence: stepark@wakehealth.edu
https://doi.org/10.1016/j.isci.2025.112584

SUMMARY

Bcl2 inhibition has excellent antitumor activity against hematologic malignancies. However, the clinical results in lymphomas harboring *BCL2* gene rearrangements have been disappointing, and the mechanism of this intrinsic resistance remains unknown. Herein, we report that Bcl2 inhibition rapidly repressed p53 with poor response in *BCL2*-rearranged lymphoma cells. However, concurrent inhibition of aurora kinase (Aurk) overcame this primary resistance to Bcl2 inhibition by restoring the p53/p21 proapoptotic axis via a post-transcriptional increase in p53. Two independent *BCL2*-rearranged lymphoma murine models showed complete tumor regression in all animals treated with combined Bcl2/Aurk inhibition, whereas mice treated with single-agents demonstrated rapid progression. Transcriptome analysis confirmed that *BCL2*-rearranged lymphomas rapidly downregulated the p53 target CDKN1A (p21) in response to Bcl2 inhibition *in vivo*. However, concurrent inhibition of Aurk restored the TP53/CDKN1A pathway, sensitizing the tumors to Bcl2 inhibitor-mediated apoptosis. These data lay the groundwork for evaluation of this combination in the clinical setting.

INTRODUCTION

Bcl2 is an antiapoptotic protein that, along with its family members, controls normal B cell maturation and mitochondrial-mediated intrinsic cell death.[1–3] Dysregulation of Bcl2 family members is a hallmark of B cell lymphoma and is clinically targeted in the treatment of many hematological malignancies.[4–6] Specifically, venetoclax, a selective and potent inhibitor of Bcl2, has shown excellent clinical activity in various types of non-Hodgkin lymphoma (NHL) and has been approved by the US Food and Drug Administration (FDA) for the treatment of relapsed or refractory chronic lymphocytic leukemia (CLL) or small lymphocytic lymphoma (SLL). However, its efficacy has mostly been disappointing in *BCL2*-rearranged lymphomas harboring classic *BCL2* gene rearrangements, including follicular lymphoma (FL), diffuse large B cell lymphoma (DLBCL), double-hit lymphoma (DHL), and triple-hit lymphoma (THL).[7] A recent clinical trial evaluating venetoclax in combination with rituximab with or without bendamustine in relapsed or refractory FL further revealed a limited clinical benefit of venetoclax in these *BCL2*-rearranged lymphomas.[8]

The mechanism by which *BCL2*-rearranged lymphomas evade Bcl2 inhibition remains largely elusive with significant clinical implications.[9,10] Studies have shown that some tumor cells, such as CLL and mantle cell lymphoma (MCL), acquire resistance to Bcl2 inhibition via upregulation of antiapoptotic proteins, such as Bcl-xL and Mcl1, which results in treatment failure after prolonged exposure to venetoclax.[11] In addition, changes in cell metabolism and mitochondrial reprogramming have been suggested to play a key role in acquired drug resistance to venetoclax in other tumor cells.[12,13] Moreover, alterations in expression and/or function of the tumor suppressor p53 have been demonstrated to induce resistance to apoptosis via Bcl2 inhibition.[13]

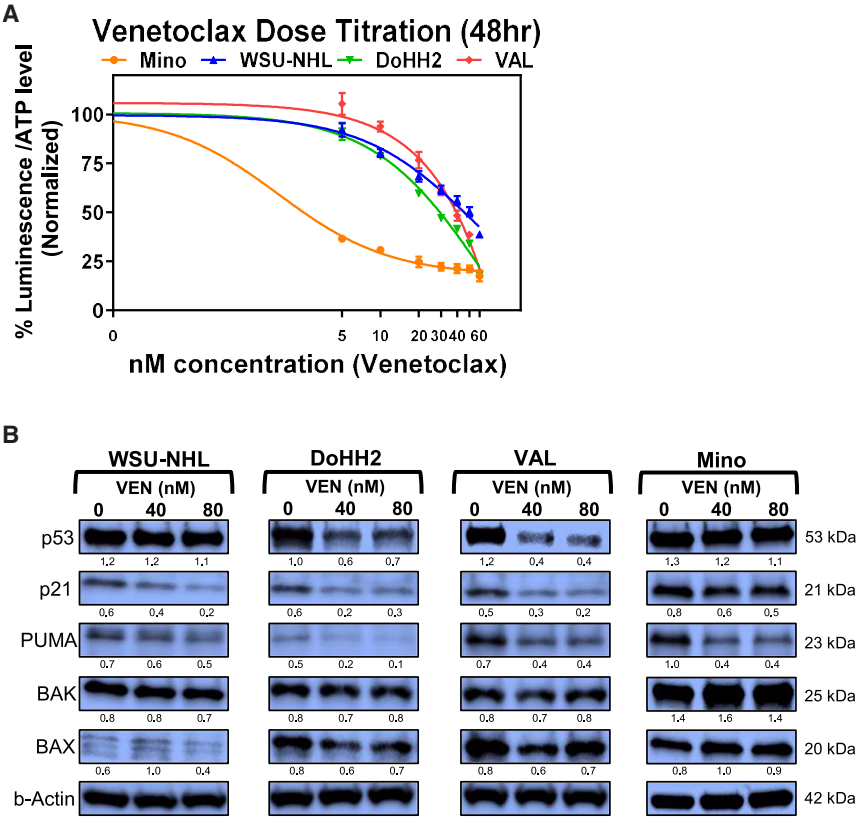

Figure 1. Venetoclax mediates repression on *TP53* and p21 in *BCL2*-rearranged lymphoma cell lines

(A) Sensitivity of *BCL2*-rearranged cell lines (WSU-NHL, DoHH2, VAL) vs. the control Mino cells to venetoclax as determined by ATP levels after indicated treatment doses and hours. ATP levels were quantified and normalized to vehicle control, and each data point is mean of triplicate wells and graphs are representative of three independent experiments. Data are represented as mean ± SD. (B) Changes in proapoptotic proteins after 24 h of venetoclax treatment in *BCL2*-rearranged lymphoma cell lines vs. the control Mino cells. Densitometric analyses of the immunoblots were preformed using ImageJ software and are listed below representative image of each target protein. The data are presented as the ratios of target protein/β-actin. Data are representative of at least two independent experiments. See also Figure S1.

Aurora kinases (Aurk) are serine/threonine kinases involved in mitotic regulation, with an additional functional role in the regulation of tumor suppressor proteins including p53, and inhibition of Aurk has been associated with the potent upregulation of proteins involved in the *TP53* proapoptotic axis.[14,15] Aurk inhibitors have been tested in clinical trials; however, the use of Aurk inhibition alone, or in combination with standard chemotherapies, has not produced improved results. Therefore, we identified Aurk as a potential druggable target to overcome primary and innate resistance to venetoclax in *BCL2*-rearranged lymphomas.

RESULTS

Venetoclax induces p53 downregulation in *BCL2*-rearranged lymphomas

To investigate the response of *BCL2*-rearranged lymphoma cells to venetoclax, we sought representative *BCL2*-rearranged lymphomas with or without concurrent rearrangements of *MYC* (*MYC*+) and/or *BCL6* (*BCL6*+) verified by fluorescence *in situ* hybridization (FISH) analysis. All *BCL2*-rearranged cell lines demonstrated increased Bcl2 protein expression compared to the control cell lines, which do not harbor BCL2 rearrangement, although they showed varying degrees of Bcl2 protein expression at baseline (Figure S1A). We selected WSU-NHL (single hit; *BCL2*+/*MYC*-/*BCL6*-), DoHH2 (DHL; *BCL2*-+/*MYC*+/*BCL6*-), and VAL (THL; *BCL2*-+/*MYC*+/*BCL6*+) and determined their sensitivity to single-agent venetoclax. Mino MCL) cells, which do not harbor *BCL2* rearrangement, were used as a reference cell line because they are known to be sensitive to venetoclax.[15,16] As expected, Mino cells were highly susceptible to venetoclax, with an IC^{50} of approximately 5 nM (Figure 1A). *BCL2*-rearranged lymphoma cells responded to venetoclax to varying degrees, but all tested *BCL2*-rearranged cell lines demonstrated inherent resistance to Bcl2 inhibition by venetoclax *in vitro*, with IC^{50} values 6- to 10-fold higher than that of Mino cells. Immunoblotting revealed that, in *BCL2*-rearranged lymphoma cells, venetoclax induced a downregulation of the *TP53*-axis, decreasing the expression of p53 and its transcriptional targets p21 and Puma (Figure 1B). The level of p53 decreased with or without Q-VD-OPh, a pan-caspase inhibitor, indicating that the protein levels did not decrease because of increased apoptosis (Figure S1B). Mcl1 and Bcl-xL remained largely unchanged in *BCL2*-rearranged lymphoma cells (Figure S1C). Based on these data, we hypothesized that the observed repression of the proapoptotic *TP53*-axis might be responsible for the primary venetoclax failure, which is well documented in *BCL2*-rearranged lymphomas.

Aurk inhibition sensitizes *BCL2*-rearranged lymphomas to venetoclax

Aurk inhibitors have been reported to be potent inducers of the *TP53*-axis in various malignancies.[14,15] Post-translational restoration or stabilization of the p53 protein via Aurk inhibition has been well documented.[17–20] Therefore, we investigated various inhibitors of Aurk to determine whether Aurk inhibition can overcome the primary failure of venetoclax by restoring the *TP53* proapoptotic axis in *BCL2*-rearranged lymphomas. *BCL2*-rearranged lymphoma cells were subsequently evaluated for viability after treatment with venetoclax with or without MLN8237 (Aurk-A inhibitor), LY3295668 (Aurk-A inhibitor), or AZD2811 (Aurk-B inhibitor). All Aurk inhibitors showed minimal to moderate cytotoxic activity in *BCL2*-rearranged lymphomas

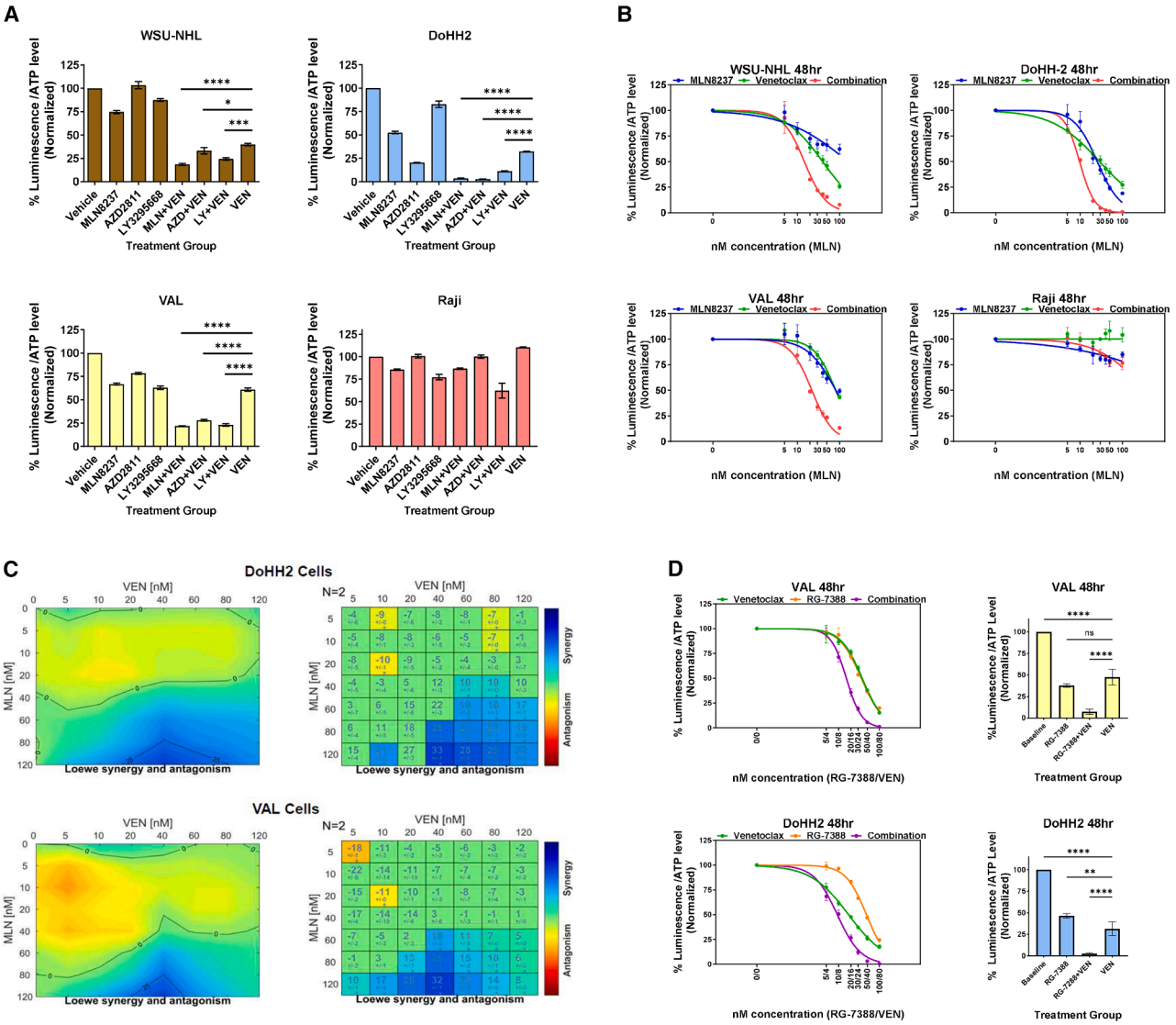

Figure 2. AURK-A, AURK-B, or MDM2 inhibitor in combination with Venetoclax induces synergism in *BCL2*-rearranged lymphoma cells

(A) Cells were treated for 48 h with MLN8237 (MLN, 50 nM), AZD2811 (AZD, 40 nM), LY3295668 (LY, 250 nM), and/or venetoclax (VEN, 40 nM) in WSU-NHL (*BCL2*+/*MYC*-/*BCL6*-), DoHH2 (*BCL2*+/*MYC*+/*BCL6*-), and VAL (*BCL2*+/*MYC*+/*BCL6*+) cells. Raji cells (*BCL2*-/*MYC*+) were shown in comparison. Statistical significance was determined by multiple unpaired t-test. Data are represented as mean ± SD.

(B) Focused cytotoxicity assays of MLN8237, venetoclax, or combination treatment in resistant *BCL2*-rearranged cells WSU-NHL, DoHH2, and VAL. *BCL2*-wild-type Raji cells were shown in comparison. ATP levels were quantified and normalized to vehicle control, and each data point is mean of triplicate wells and graphs are representative of three independent experiments. Data are represented as mean ± SD.

(C) Synergism analysis using Combenefit in DoHH2 and VAL cells.

(D) Focused cytotoxicity assays of venetoclax, RG-7388, or combination treatment of VEN+RG-7388 in VAL and DoHH2. Cells were treated for 48 h with RG-7388 (50 nM), venetoclax (40 nM), or combination (50 nM RG-7388/40 nM VEN) in VAL and DoHH2 cells. Values are normalized and an average of three independent experiments. Statistical significance was determined by one-way ANOVA with multiple comparisons. Data are represented as mean ± SD. (****$p < 0.0001$, ***$p < 0.001$, **$p < 0.01$, and *$p < 0.05$). See also Figures S3 and S4.

(Figures 2A and 2B). Notably, when an Aurk inhibitor was combined with venetoclax, significant synergistic effects were observed compared to treatment with single agents alone ($p < 0.0001$). The combination index (CI) values were less than 1 at various concentrations, indicating that the combinations were highly synergistic. Two additional NHL cells harboring *BCL2* rearrangements, SU-DHL-4 and SU-DHL-6, were tested with the VEN+MLN8237 combination, with viability assays confirming the synergistic effects observed in the other *BCL2*-rearranged lymphomas (Figures S4A and S4B). Conversely, venetoclax had no significant cytotoxic activity in *BCL2*-/*MYC*+ Raji or Ramos cells,[21] which lack *BCL2* rearrangements; the incorporation of an Aurk inhibitor with venetoclax had minimal to no additive or synergistic effects on Raji (Figures 2A and 2B) or Ramos

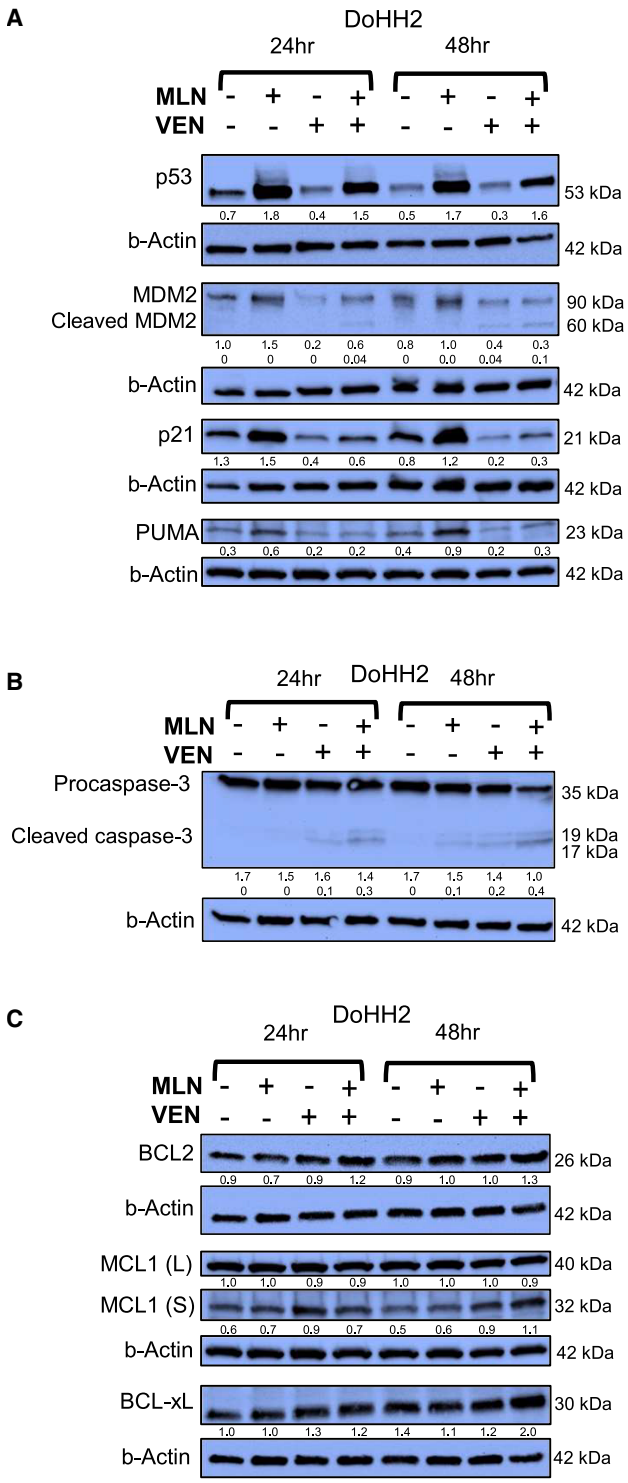

Figure 3. MLN8237 induces p53 and p21 expression in *BCL2*-rearranged lymphoma cells

(A–C) Immunoblotting of cell lysates for p53 and its target proteins in *BCL2*-rearranged lymphoma cells (A) Effect of MLN8237 (MLN, 50 nM) and venetoclax (VEN, 40 nM) on p53, its downstream targets, and MDM2 protein expression in DoHH2.

(data not shown) cells. Synergism analysis using Combenefit[22] revealed that the combination of venetoclax and MLN8237 (VEN+MLN8237) at a 4:5 ratio induced profound synergistic cytotoxic activity in tested *BCL2*-rearranged lymphoma cells (Figure 2C). Mdm2 inhibition, another pathway with the potential to restore the *TP53*-axis, was also evaluated. RG-7388, an Mdm2 inhibitor, showed similar synergistic effects when combined with venetoclax, further supporting the importance of the *TP53*-axis in overcoming primary resistance to venetoclax in *BCL2*-rearranged lymphoma (Figure 2D). In contrast, Mcl1 inhibition by S63485 did not show any significant cytotoxic effects on *BCL2*-rearranged lymphoma cells as a single agent or in combination with venetoclax, consistent with the western blot data demonstrating no change in Mcl1 expression (Figure S2). The proapoptotic effect of VEN+MLN8237 was further assessed using annexin-V assays, and these data confirmed that the combination treatment led to increased levels of apoptosis in *BCL2*-rearranged lymphoma cells (Figure S3). Based on these data and the robust preclinical and clinical data available on MLN8237,[23–25] the VEN+MLN8237 combination was chosen for further in-depth analysis.

Aurk inhibition reverses *TP53*-axis repression and induces biphasic G0/G1 and G2/M cell-cycle arrest in *BCL2*-rearranged lymphomas

Bcl2 inhibition by venetoclax was associated with the downregulation of the *TP53*-axis in *BCL2*-rearranged cells as early as 6 h post-exposure (Figure S5A), corroborative with previous reports on the direct role of *TP53* in mitochondrial cell death.[26,27] Venetoclax had no significant effect on *TP53*-axis in the control Raji cells, which lack *BCL2* rearrangement. Although MLN8237 alone did not induce significant cytotoxicity (Figure 2), it was associated with marked upregulation of the *TP53*-axis in *BCL2*-rearranged lymphoma cells (Figures 3A, S5A, S5B, and S6A). This effect was evident both as a single agent and in combination with venetoclax. MLN8237 treatment also led to the upregulation of the p53 regulator Mdm2 (Figures 3A, S5A, S5B and S6A). Moreover, transcriptional targets of p53 were upregulated by treatment with MLN8237. In both DoHH2 and VAL cell lines, which carry the wild-type *TP53* gene, p21 protein levels increased markedly after treatment with MLN8237 (Figures 3A and S5B). PUMA, another direct target of *TP53*, was induced by MLN8237 in *BCL2*-rearranged lymphomas, including DOHH2 and WSU-NHL cells (Figure S6B). The induction of p53 and p21 by other Aurk inhibitors was also observed (Figure S6C). Immunoblotting for caspase-3 cleavage in DoHH2 cells treated with the VEN+MLN8237 combination showed more substantial cleavage and activation of caspase-3 compared to groups treated with either agent alone (Figure 3B). Notably, Myc

(B) Effect of MLN8237 (50 nM) and venetoclax (40 nM) on caspase-3 cleavage. (C) Effect of MLN8237 (50 nM) and venetoclax (40 nM) on antiapoptotic Bcl2 family member proteins. Please note, PUMA (A) and MCL1 L and S (C) were run on the same gel and thus share the same β-actin loading control. Densitometric analyses of the immunoblots were performed using ImageJ software and are listed below representative image of each target protein. The data are presented as the ratios of target protein/β-actin. Data are representative of at least two independent experiments. See also and Figures S2, S5, S6, S7, S8.

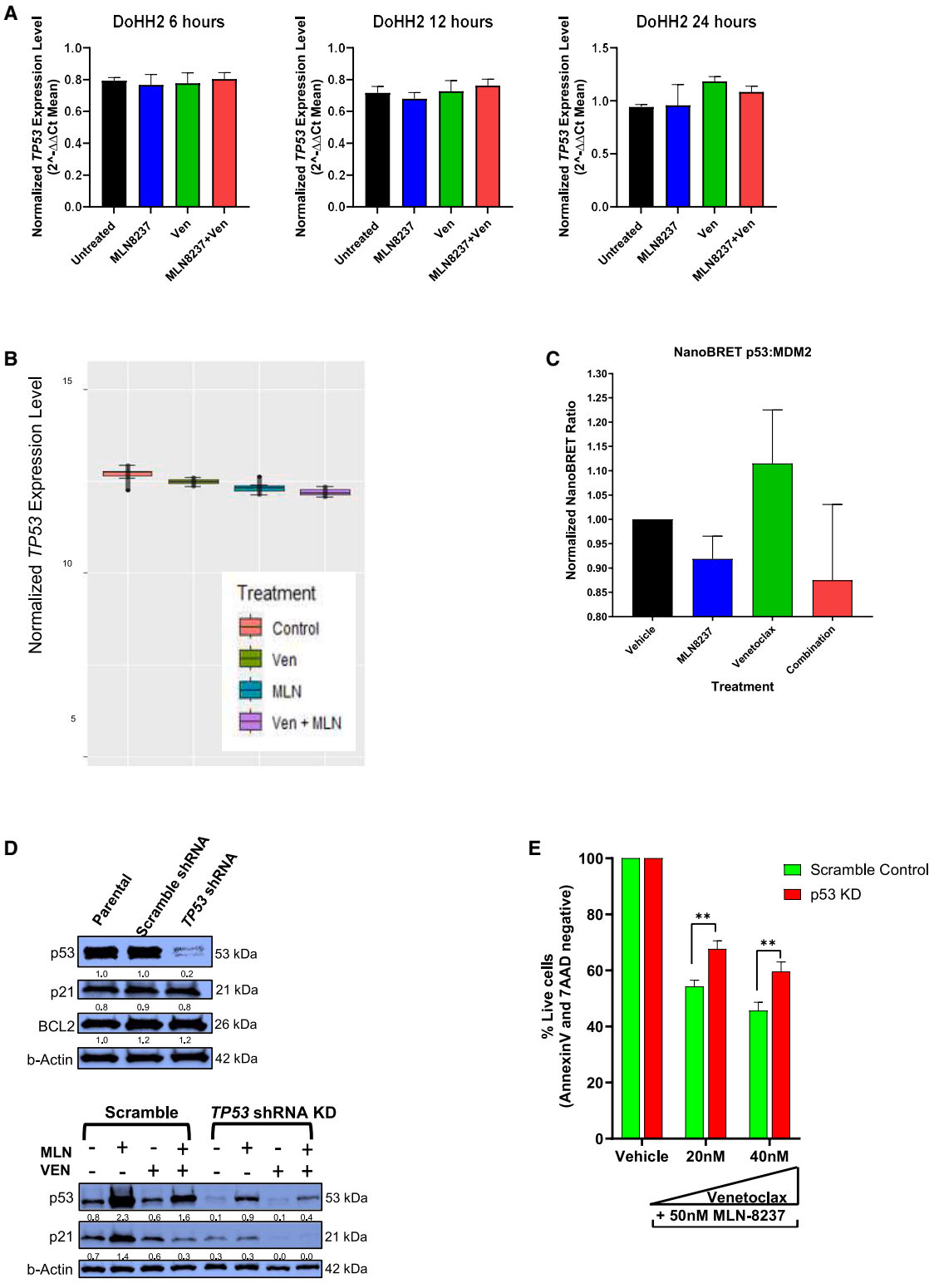

Figure 4. MLN8237 upregulates p53-axis via stabilization of p53 post-translationally

(A) RT-qPCR detection of *TP53* mRNA in venetoclax (VEN, 40 nM), MLN8237 (MLN, 50 nM), or VEN+MLN combination treated DoHH2 cells at 6, 12, and 24 h time points. No significant changes in *TP53* mRNA levels observed at any of the time points with any of the treatment groups, indicating no changes in *TP53* expression at the transcriptional level. Data are represented as mean ± SD.

(legend continued on next page)

degradation occurred much later (~48 h) after treatment with MLN8237 or in combination (Figure S7A). There was no decrease in *MYC* mRNA observed in tumors from MLN8237 treated mice (Figure S7B), implying that the *TP53* upregulation preceded *MYC* downregulation induced by Aurk inhibition, and *MYC* likely had no major role during the early stage of rapid tumor cell killing by the VEN+MLN8237 combination. As previously reported, venetoclax had no direct impact on Bcl2 protein expression, and we further extended this finding to Bcl-xL (Figure 3C).

In addition, we evaluated the effects of Bcl2 and Aurk inhibition on the cell cycle in *BCL2*-rearranged lymphomas. As p21 expression is strongly related to G1 cell-cycle arrest,[28,29] we tested the DNA content of *BCL2*-rearranged cells treated with MLN8237, venetoclax, or VEN+MLN8237 for cell cycle analysis. Interestingly, *BCL2*-rearranged lymphoma cells showed minimal to no shift to G2/M phase with no evidence of polyploid cells when treated with MLN8237 at 50 nM (Figure S8). This was an interesting finding because MLN8237 had a profound effect on DNA content and polyploidy in Raji cells at the same concentration (Figure S8C). Notably, higher concentrations of MLN8237 (≥200nM) led to a more traditional G2/M arrest in *BCL2*-rearranged lymphoma cells (Figure S8). Thus, MLN8237 induced biphasic G0/G1 and G2/M arrest at different concentrations in *BCL2*-rearranged lymphomas. In the current study, enhanced G0/G1 arrest via upregulation of p21 could also be responsible for priming *BCL2*-rearranged lymphomas to venetoclax, which mediates apoptosis in the G0/G1 phase.[18,30]

Aurk inhibition upregulates *TP53*-axis via stabilization of p53

To determine whether *TP53* downregulation by *BCL2*-rearranged lymphomas occurs through transcriptional or post-translational mechanisms upon first exposure to venetoclax, we evaluated *TP53* mRNA transcript levels in response to therapy. Real-time reverse-transcription PCR (RT-PCR) on *in vitro* samples and RNA sequencing (RNA-seq) analysis of *in vivo* treated tumors showed no significant changes in *TP53* mRNA expression levels in response to venetoclax, MLN8237, or VEN+MLN combination (Figures 4A and 4B, respectively), indicating that venetoclax-induced *TP53*-axis downregulation in *BCL2*-rearranged lymphoma does not occur at the transcriptional level of *TP53*. Aurk is known to be involved in the regulation of the *TP53*-axis through phosphorylation-mediated post-translational modification of the p53 protein, and inhibition of Aurk has been shown to increase p53 protein levels in some tumor cells.[19,31] To further confirm that Aurk inhibition restores *TP53*-axis function post-translationally, we performed a bioluminescence resonance energy transfer (BRET) assay to evaluate the p53:Mdm2 protein-protein interaction in response to venetoclax, MLN8237, or VEN+MLN combination. Treatment with venetoclax enhanced the interaction between p53 and Mdm2, which is responsible for the increased degradation of p53 (Figure 4C). Conversely, MLN8237 decreased the interaction between p53 and Mdm2 both as a single agent and in combination with venetoclax. MLN8237, when combined with venetoclax, reversed the enhanced p53:Mdm2 interaction observed in *BCL2*-rearranged lymphoma cells treated with venetoclax alone.

TP53 knockdown abrogates the synergistic effect of VEN+MLN8237 combination

We subsequently generated *TP53*-knockdown DoHH2 cells using TP53 shRNA to further identify the role of *TP53*-axis in VEN+MLN8237 combination. Immunoblotting revealed a robust reduction in p53 protein in the knockdown cells, while no significant changes were noted in scrambled shRNA control cells, confirming the effective knockdown of *TP53* by shRNA with near-complete abrogation of p53 expression (Figure 4D). Notably, no changes in Bcl2 and p21 proteins were observed in *TP53*-knockdown DoHH2 cells compared with parental cells. Cytotoxicity assays demonstrated that *TP53*-knockdown abrogated the synergistic effect of VEN+MLN8237 combination (Figure 4E). Addition of MLN8237 to venetoclax failed to induce p53/p21 in *TP53*-knockdown cells, further supporting the importance of the intact *TP53*-axis in overcoming primary resistance to Bcl2 inhibition in *BCL2*-rearranged tumors (Figure 4D). VEN+MLN8237 combination was effective in all tested cells with *BCL2*-rearrangement irrespective of their *TP53* mutational status although the sensitivity of the combination was attenuated in some cells containing mutated *TP53* (Table S1), indicating that the mutated *TP53* can be rescued as long as they do not have loss-of-function mutations (Figure S4). These data collectively suggest that induction of the *TP53*-axis directly sensitizes *BCL2*-rearranged lymphoma cells to venetoclax, which provides the basis for the synergism between venetoclax and MLN8237.

VEN+MLN8237 combination induces rapid and complete regression of *BCL2*-rearranged tumors *in vivo*

To test the efficacy of VEN+MLN8237 combination in *BCL2*-rearranged lymphoma cells, we first used a *BCL2*-rearranged lymphoma subcutaneous (SC) xenograft model harboring DoHH2 cells. The mean tumor volume of vehicle-treated control mice was 1,420 mm^3 on day 16 after treatment initiation (Figure 5A). Mice receiving single-agent MLN8237 or venetoclax showed a modest delay in tumor progression, with mean tumor volumes

(B) *TP53* mRNA levels based on RNA-seq of DoHH2 cells treated with venetoclax, MLN8237, or VEN+MLN8237 combination for 72 h. Data are represented as mean ± SD.

(C) NanoBRET in COS-7 cells expressing p53 HaloTag and NanoLuc Mdm2 treated with vehicle, MLN8237 50 nM, venetoclax 40 nM, or VEN+MLN combination. Cells treated with venetoclax exhibit an increase in p53:Mdm2 interaction evidenced by an increased BRET signal, while MLN8237 and VEN+MLN treated cells demonstrate a decreased p53:Mdm2 interaction. Data are represented as mean ± SD.

(D) Immunoblots showing p53 knockdown in DoHH2 cells mediated by *TP53* shRNA. Bcl2 and p21 levels are unaffected. Scramble shRNA transduced cell line is used as control.

(E) Effect of MLN8237 (50 nM) and venetoclax (40 nM) on *TP53* KD DoHH2 cells viability. Statistical significance was determined by multiple paired t test where $^{**}p < 0.01$. Data are represented as mean ± SEM. Densitometric analyses of the immunoblots were performed using ImageJ software and are listed below representative image of each target protein. The data are presented as the ratios of target protein/β-actin. Data are representative of at least two independent experiments.

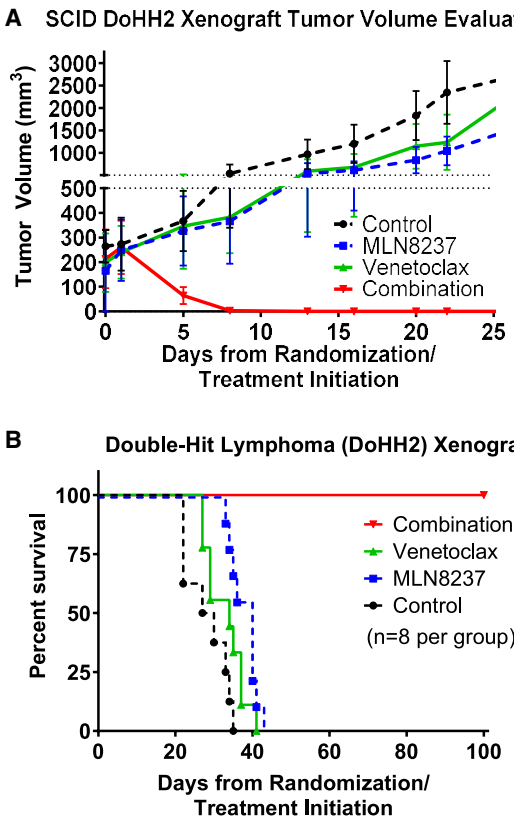

Figure 5. Venetoclax plus MLN8237 combination effectively induces complete tumor regression in *BCL2*-rearranged xenografted lymphoma model

(A) Combination therapy with venetoclax and MLN8237 induced complete tumor regression in SCID mice xenografted with *BCL2*-rearranged DoHH2 tumor cells after 3 weeks (15 days) of treatment. Data are represented as mean ± SEM.

(B) Tumor-free survival of mice treated with MLN8237 plus venetoclax combination. Animals were monitored for 80 days after the end of treatment. Statistical significance was determined by survival curve comparison with log rank (Mantel-Cox) test (n = 8 per group; ****$p < 0.0001$). See also Figures S9 and S12.

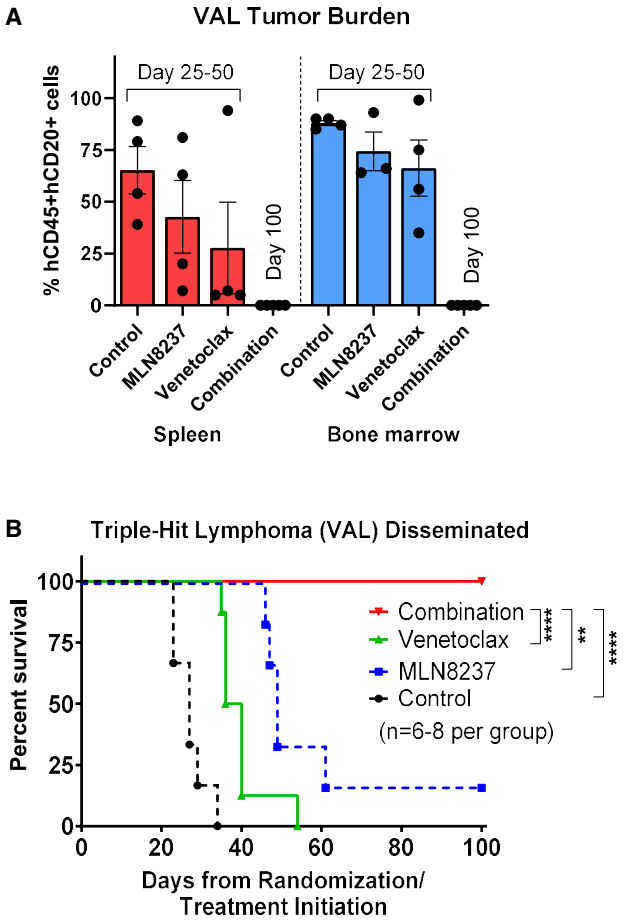

Figure 6. Venetoclax plus MLN8237 combination effectively clears disseminated *BCL2*-rearranged lymphoma model with no evidence of minimal residual disease

(A) *BCL2*-rearranged VAL tumor burden in spleen and bone marrow of NCG mice at the end of follow-up (vehicle, MLN8237, or venetoclax monotherapy) or at day 100 (venetoclax plus MLN8237 combination group). Presence of human $CD45^+CD20^+$ indicates engraftment and dissemination of tumor cells. Data are represented as mean ± SEM.

(B) Survival curves of mice harboring disseminated tumors, treated with vehicle, MLN8237, venetoclax, or the combination. One mouse (†) in the MLN8237 monotherapy group on day 100 was found to have a bulky abdominal tumor mass at the time of sacrifice. Statistical significance was determined by survival curve comparison with log rank (Mantel-Cox) test (n = 6–8 per group; ****$p < 0.0001$ and **$p < 0.01$). See also Figures S10, S11, and S12.

of 283 mm^3 and 460 mm^3, respectively, on day 16. In contrast, VEN+MLN8237 combination was associated with rapid tumor regression within seven days of treatment, with a median tumor volume of 0 mm^3 on day 16. The differences in tumor volumes were statistically significant between the combination group and the groups treated with either agent alone ($p < 0.02$). Tumor volume differences translated to significantly improved survival rates with a 100-day survival rate of 100% (n = 8) in mice treated with VEN+MLN8237 combination ($p < 0.0001$), while mice in all other groups were euthanized by day 45 due to tumor progression (Figure 5B). There was no significant toxicity associated with the VEN+MLN8237 combination based on the recorded body weight in animals (Figure S9A).

The combined therapeutic approach was next evaluated in a more aggressive disseminated *BCL2*-rearranged lymphoma model. NCG mice were intravenously injected with *BCL2*-rearranged VAL cells via the tail vein to create widely disseminated tumors. As seen in the SC xenograft model, VEN+MLN8237 combination rapidly cleared disseminated VAL lymphoma cells and led to complete remission in all (n = 8) treated mice, as evidenced by the absence of CD20+/CD45+ cells in the spleen and bone marrow by flow cytometric analysis (Figures 6A and S10A). In contrast, all mice in the control or single-agent groups showed evidence of disease progression at the time of tissue collection. Notably, the one surviving mouse in the MLN8237 group had a bulky abdominal tumor mass, while all mice in VEN+MLN8237 combination group showed no evidence of minimal residual disease documented by flow cytometric analysis with a tumor-free survival rate of 100% on day 100 ($p < 0.0001$, Figure 6B). Similar

to the CB17-SCID SC xenograft model, none of the NCG mice receiving VEN+MLN8237 combination displayed signs of weight loss throughout the course of the study (Figure S9B), and no evidence of hind limb paralysis was present in the combination group. Lastly, the serum complete metabolic panel evaluating the renal and hepatic functions, as well as histopathology of the normal organs, further demonstrated that VEN+MLN8237 combination was not associated with any discernible toxicity in the treated animals (Figures S10A, S10B, and S11). Additionally, the safety of VEN+MLN8237 combination was evaluated in an immunocompetent BALB/c mouse model using complete blood counts, a complete metabolic panel, and a T cell repertoire panel by flow cytometry. VEN+MLN8237 combination was not associated with any significant hematological, renal, or hepatic toxicity after 2, 4, and 8 weeks of treatment in immunocompetent mice (Figure S12A). Flow cytometric analysis of T cell populations showed no dramatic changes in the T cell repertoire with stable $CD4^+$ and regulatory T cells, although there was a mild decrease in $CD8^+$ T cells after treatment with VEN+MLN8237 (Figure S12B). Taken together, these data indicate that the combination of VEN+MLN8237 results in synthetic lethality *in vivo* and leads to the rapid and complete regression of *BCL2*-rearranged lymphomas with no discernible toxicity across animal models.

Next generation sequencing identifies transcriptome changes in response to venetoclax and MLN8237 in *BCL2*-rearranged lymphoma

A sub-study xenograft experiment was performed to evaluate changes in mRNA expression in response to venetoclax, MLN8237, or VEN+MLN8237 combination *in vivo*, and tumors were collected after 3 days of treatment with venetoclax, MLN8237, or VEN+MLN8237 combination. The tumors treated with venetoclax monotherapy demonstrated 37 differentially expressed genes (fold-change >2 and FDR <0.05) in comparison with the vehicle control (Figure 7A). The comparison between venetoclax and VEN+MLN8237 resulted in the identification of 43 genes that were differentially expressed (fold change>2 and FDR <0.05), as shown in the volcano plot (Figure 7B). We then filtered genes from venetoclax and VEN+MLN8237 combination groups to identify the genes that were bidirectional in venetoclax and the combination. This analysis yielded 41 genes, of which 33 were upregulated and eight were downregulated in VEN+MLN8237 combination group. Most notably, *CDKN1A* (p21) transcript levels were decreased by > 2-fold in venetoclax monotherapy compared to the vehicle control, while the concurrent inhibition of Aurk-A by MLN8237 upregulated *CDKN1A* (p21) expression by > 4-fold compared to the venetoclax monotherapy group. Notably, *CDKN1A* was one of the most significantly upregulated genes in MLN8237 monotherapy compared to that in the control ($p < 0.05$, data not shown). Ingenuity pathway analysis revealed that the combination of VEN+MLN8237 induced marked upregulation of the *TP53*/p21-axis (Figure 7C). The data also showed upregulation of *BAX* mRNA expression *in vivo*, in agreement with previous *in vitro* data showing an increased level of Bax associated with VEN+MLN8237 combination (Figure S5B). A comprehensive analysis of tumors treated with VEN+MLN8237 combination revealed upregulation of the *TP53* axis-associated genes *CDKN1A* (p21), *BBC3* (PUMA), *DDB2*, *BTG2*, *TRIM22*, *PLXNB2*, and *BAX*. Of note, there were no significant differences in *MYC* mRNA expression in the single drug treatment arms although there was a slight decrease in *MYC* mRNA in the combination group (Figure S7B). However, the timing of *MYC* downregulation happened at a much later time point (>48 h), which was outside the window for the observed synergistic effect as shown in previous experiments *in vitro*.

DISCUSSION

Venetoclax has emerged as an integral part of cancer therapy in various hematologic malignancies; however, intrinsic and acquired resistance to Bcl2 inhibition remains a major obstacle in advancing this promising therapeutic approach.[9,32] The lack of expected efficacy in *BCL2*-arranged lymphomas has been especially disappointing, and the mechanism by which *BCL2*-rearranged lymphomas evade Bcl2 inhibition has remained largely unknown, although the potential mechanisms of secondary or acquired resistance to venetoclax have been extensively studied in other tumor types, such as CLL, MCL, and acute myeloid leukemia (AML). One of the central mechanisms of acquired resistance to venetoclax involves alterations in the members of the apoptotic machinery, such as Bcl-xL and Mcl1,[33,34] and acquisition of genetic mutations in $BCL2^{G101V \text{ or } D103Y}$ has been associated with reduced binding affinity of the Bcl2 protein after prolonged exposure to venetoclax in CLL cells.[35–37] However, more recently, studies on AML and CLL have highlighted the role of the *TP53* network in acquired resistance to venetoclax.[12,13,38,39] In this study, we investigated the mechanism of intrinsic resistance to Bcl2-inhibition in *BCL2*-rearranged lymphomas. Our study demonstrates that *BCL2*-rearranged lymphomas evade Bcl2 inhibition via rapid and profound downregulation of the *TP53*-axis.

Dysregulation of the *TP53*-axis occurs in various cancers, including lymphoid malignancies.[40] While levels of p53 can determine if cells undergo cell-cycle arrest or cellular apoptosis after stress, the apoptotic threshold is largely elevated in many tumor cells via aberrant expression of *TP53*.[41,42] Our transcriptome analyses with venetoclax-treated *BCL2*-rearranged lymphoma revealed near-immediate and profound repression of the *TP53*-axis, including *CDKN1A* (p21). Guieze et al. investigated the mechanism of acquired resistance to Bcl2 inhibition in CLL, and primarily, they demonstrated the role of mitochondrial reprogramming in resistance to Bcl2 inhibition. Moreover, RNA-seq analysis of *BCL2*-rearranged OCI-Ly1 lymphoma cells from the same study showed that *CDKN1A* was one of the most downregulated genes in venetoclax-resistant tumor cells compared to those sensitive to venetoclax.[13] Although this finding was not further investigated, the data support our findings that *CDKN1A* (p21) is significantly downregulated in *BCL2*-rearranged tumors in response to venetoclax. In addition, there is increasing evidence that *TP53* downregulation may play a critical role in resistance to Bcl2 inhibition in AML. Nechiporuk et al. identified *TP53* as one of the key genes involved in venetoclax resistance in AML cells, suggesting that inactivation of *TP53* led to resistance to venetoclax. In addition, AML patient samples

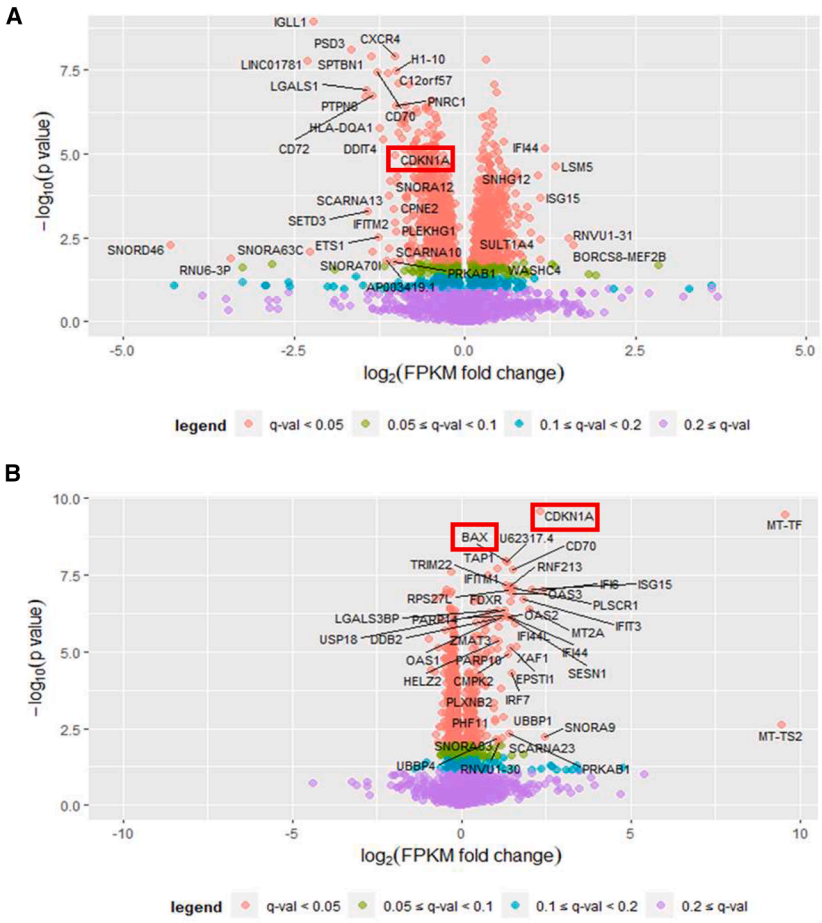

Red = Increased expression
Green = Decreased expression

Figure 7. RNA sequencing of *BCL2*-rearranged tumor grafts identifies transcriptome changes driven by BCL2 and/or AURK inhibition

(A) Volcano plot showing differential transcriptome expressions between vehicle (reference) and venetoclax (VEN) monotherapy.

(B) Volcano plot showing differential transcriptome expressions between venetoclax monotherapy (reference) and venetoclax plus MLN8237 (MLN) combination therapy.

(C) Ingenuity pathway analysis showing p21 (*CDKN1A*) as the primary network differentially affected in the venetoclax plus MLN8237 combination group. Red indicates increase and green indicates decrease in mRNA levels in the tumor grafts. See also and Figures S5, S6, S7.

with low p53 expression were associated with increased resistance to venetoclax.[12] Likewise, our *TP53*-knockdown model showed that an intact *TP53*-proapoptotic axis is critical for overcoming primary resistance to venetoclax in *BCL2*-rearranged lymphomas. However, unlike previous leukemia studies,[18,38] ours did not identify any significant changes in Bak or Mcl1 expression levels in resistant *BCL2*-rearranged lymphoma cells. The resistance mechanisms are likely heterogeneous in different tumor types with inactivation of the *TP53*-proapoptotic axis functioning as the common denominator in resistance to venetoclax.

TP53 is an attractive target for anticancer therapy because of its function in cellular responses to various oncogenic stimuli, including the cell cycle, apoptosis, and senescence.[43,44] Many transcriptional and post-transcriptional mechanisms maintain tight regulatory control of *TP53* expression, including the TP53: Mdm2 interaction, and targeting these pathways to counteract *TP53*-axis inactivation has therapeutic potential. Although there are a few p53 activators and Mdm2 inhibitors in preclinical or early clinical stages of development,[45,46] our *in vitro* data indicated that Mdm2 inhibition can overcome resistance to venetoclax. To date no effective therapy against tumors with aberrant *TP53* has been proven in phase 3 clinical trials. Aurks, a family of serine/threonine kinases, control mitotic regulation, and inhibition of Aurk has been shown to result in cell-cycle arrest in the G2/M phase with formation of polyploid cells and cellular death.[14,28,29,45–47] Aurk inhibition is also known as one of the most potent methods for increasing p53 expression in various tumors.[14,15,48–50] Aurk can directly inhibit DNA binding and transactivation activity of p53 in a Ser-215 phosphorylation-dependent manner and reduce expression of *TP53* downstream targets.[51] The Mdm2-mediated degradation of phosphorylated p53 by Aurk-A/B has also been reported.[19,20] More recently, Aurks and p53 were shown to counteract each other by disrupting the protein stabilization process.[52] Moreover, small-molecule inhibitors against Aurks are in advanced stages of clinical development, thus making these molecules excellent candidates for restoring p53 expression in *BCL2*-rearranged tumors with innate resistance to Bcl2 inhibition.[24,25] The safety of MLN8237, a small molecule AurkA inhibitor, has been vigorously tested in advanced phase clinical trials, including multiple randomized phase 2 and 3 trials, with no evidence of unexpected toxicity as a single agent or in combination with other targeted therapy and chemotherapy drugs.[23–25] Hence, MLN8237 is an excellent candidate for drug repurposing, especially when used in combination with other targeted small-molecule inhibitors.

Our data demonstrated that inhibition of Aurk induces potent activation of proapoptotic proteins involved in the *TP53*-axis in *BCL2*-rearranged lymphomas, similar to previous reports in solid tumors and multiple myeloma.[14,15] Importantly, Aurk inhibition effectively counteracted the observed p53 repression in *BCL2*-rearranged lymphomas in response to venetoclax. This was further supported by our RNA-seq data on *BCL2*-rearranged tumors harvested from mice treated with venetoclax vs. VEN +MLN8237 combination. Specifically, there was a > 4-fold increase in *CDKN1A* expression and restoration of the *TP53*/p21 axis in *BCL2*-rearranged lymphoma cells treated with VEN +MLN8237 compared to venetoclax monotherapy. *BCL2*-rearranged lymphoma cells were extremely sensitive to VEN +MLN8237 combination, as previously shown by Kong et al. in double-hit lymphoma.[53] This is also in agreement with the data presented by Pan et al., who showed synthetic lethality of combined p53 activation and Bcl2 inhibition in AML.[18] The current study indicates that resistant cells become highly dependent on *TP53* downregulation for survival after Bcl2 inhibition, and the reversal of this process by Aurk inhibition leads to synthetic lethality in *BCL2*-rearranged lymphomas. Our data also showed increased Bax expression in response to VEN+MLN8237 combination; thus, both p21 and Puma/Bax, the two major downstream pathways of p53, may play a key role in the synthetic lethality. The relative contribution of p21 and Bax to the synergistic interaction between Bcl2 and Aurk-inhibition remains unclear and needs to be further elucidated in future studies. In addition, VEN+MLN8237 combination was effective even in *TP53* mutated cells although *TP53* knockdown abrogated the synergistic effect of this combination, suggesting that the mutated *TP53* can be rescued as long as they do not have loss-of-function mutations. In the current study, the combination of VEN+MLN8237 induced rapid and complete regression of tumors and led to long-term tumor-free survival in all treated animals in two independent *BCL2*-rearranged lymphoma models. In addition, VEN+MLN8237 combination was well tolerated, with no discernible toxicity in multiple animal models, including immunocompetent mice.

In summary, our data demonstrate that *BCL2*-rearranged lymphomas respond to Bcl2 inhibition via rapid and profound downregulation of the *TP53*-axis, responsible for their primary refractory nature to venetoclax. This offers a plausible explanation for the relative lack of clinical activity associated with venetoclax in *BCL2*-rearranged lymphomas, including FL and DLBCL. Concurrent inhibition of Aurk effectively restores the *TP53*-proapoptotic axis in resistant tumor cells, priming *BCL2*-rearranged lymphomas to be extremely sensitive to the combined Bcl2 and Aurk inhibition. Furthermore, VEN+MLN8237 combination demonstrated excellent efficacy and favorable toxicity profiles in multiple *BCL2*-rearranged animal models, thus laying the groundwork for further evaluation of this combination in the clinical setting.

Limitations of the study

The mechanisms underlying the Bcl2-inhibition-driven regulation of p53 expression remain incompletely understood, and further investigation is needed. Although *in vitro* and *in vivo* models showed very promising results, these models cannot fully reproduce the complexity of human physiology. As such, while this combination of Bcl2 and Aurk inhibition shows potential as a therapeutic approach, its clinical safety and efficacy in humans require clinical trials. Despite these limitations, our findings suggest that the combination of Bcl2 and Aurk inhibition could serve as an important tool for the treatment of high-risk lymphoma.

RESOURCE AVAILABILITY

Lead contact

Requests for further information and resources should be directed to and will be fulfilled by the lead contact, Dr. Steven I. Park (steven.park@atriumhealth.org).

Materials availability

Plasmids generated during this study are available upon request from Dr. Steven I. Park (steven.park@atriumhealth.org).

Data and code availability

- RNA-seq data have been deposited at Gene Expression Omnibus (GEO) with GEO accession # GSE200410 and are publicly available as of 12-31-24.
- This study did not generate original code.
- Any additional information required to reanalyze the data reported in this paper is available from the lead contact upon request.

ACKNOWLEDGMENTS

Steven I. Park, MD, was supported by an American Cancer Society-Kirby Foundation Mission Boost Grant (MBG-21-069-01-MBG), American Cancer Society-Mentored Research Scholar Grant in Tumor Biology and Genomics (126601-MRSG-14-215-01-TBG), and Leukemia Lymphoma Society Translational Research Program, Follicular Lymphoma Foundation, and Institute for Follicular Lymphoma Innovation Grant (LLS-TRP- 6700-25). This study was also supported by the Leon Levine Foundation. The authors wish to acknowledge the support of the Atrium Health Wake Forest Baptist Comprehensive Cancer Center the LCI Immune Monitoring Core Laboratory, Molecular Biology Core Laboratory, Center for Biostatistics, and Canon Research Center vivarium Shared Resources, supported by the National Cancter Institute's Cancer Center Support Grant award number P30CA012197. We thank these facilities for their help with data acquisition, analysis, and providing scientific input. The content is solely the responsibility of the authors and does not necessarily represent the official views of the National Institutes of Health.

AUTHOR CONTRIBUTIONS

R.M., L.J.D., and S.I.P. designed the study, analyzed the data, and drafted the manuscript; R.M., S.B., S.L.S, M.D.T., S.E.T., and S.C.J. performed the research and contributed to data analysis; D.P., H.-T.Y., L.J.D., D.M.F., N.M. S., N.G., E.A.C., and B.R.A. contributed to the interpretation of the research; S.I.P. contributed to the conception, design, analysis, and interpretation of the research; all authors reviewed and revised the manuscript.

DECLARATION OF INTERESTS

Steven I. Park reports receiving research funding from Seattle Genetics, Teva, Takeda, and BMS, membership on the Board of Directors or advisory committee for Epizyme, Rafael Pharmaceuticals, BMS, ADC Therapeutics, and Teva (advisory boards).

STAR★METHODS

Detailed methods are provided in the online version of this paper and include the following:

SUPPLEMENTAL INFORMATION

Supplemental information can be found online at https://doi.org/10.1016/j.isci.2025.112584.

Received: January 31, 2024
Revised: December 4, 2024
Accepted: March 29, 2025
Published: May 2, 2025

REFERENCES

1. Hockenbery, D., Nuñez, G., Milliman, C., Schreiber, R.D., and Korsmeyer, S.J. (1990). Bcl-2 is an inner mitochondrial membrane protein that blocks programmed cell death. Nature *348*, 334–336. https://doi.org/10.1038/348334a0.
2. Bissonnette, R.P., Echeverri, F., Mahboubi, A., and Green, D.R. (1992). Apoptotic cell death induced by c-myc is inhibited by bcl-2. Nature *359*, 552–554. https://doi.org/10.1038/359552a0.
3. Veis, D.J., Sorenson, C.M., Shutter, J.R., and Korsmeyer, S.J. (1993). Bcl-2-deficient mice demonstrate fulminant lymphoid apoptosis, polycystic kidneys, and hypopigmented hair. Cell *75*, 229–240. https://doi.org/10.1016/0092-8674(93)80065-m.
4. Souers, A.J., Leverson, J.D., Boghaert, E.R., Ackler, S.L., Catron, N.D., Chen, J., Dayton, B.D., Ding, H., Enschede, S.H., Fairbrother, W.J., et al. (2013). ABT-199, a potent and selective BCL-2 inhibitor, achieves antitumor activity while sparing platelets. Nat. Med. *19*, 202–208. https://doi.org/10.1038/nm.3048.
5. Adams, C.M., Clark-Garvey, S., Porcu, P., and Eischen, C.M. (2018). Targeting the Bcl-2 Family in B Cell Lymphoma. Front. Oncol. *8*, 636. https://doi.org/10.3389/fonc.2018.00636.
6. Delbridge, A.R.D., Grabow, S., Strasser, A., and Vaux, D.L. (2016). Thirty years of BCL-2: translating cell death discoveries into novel cancer therapies. Nat. Rev. Cancer *16*, 99–109. https://doi.org/10.1038/nrc.2015.17.
7. Lew, T.E., and Seymour, J.F. (2022). Clinical experiences with venetoclax and other pro-apoptotic agents in lymphoid malignancies: lessons from monotherapy and chemotherapy combination. J. Hematol. Oncol. *15*, 75. https://doi.org/10.1186/s13045-022-01295-3.
8. Zinzani, P.L., Flinn, I.W., Yuen, S.L.S., Topp, M.S., Rusconi, C., Fleury, I., Le Dû, K., Arthur, C., Pro, B., Gritti, G., et al. (2020). Venetoclax-rituximab with or without bendamustine vs bendamustine-rituximab in relapsed/refractory follicular lymphoma. Blood *136*, 2628–2637. https://doi.org/10.1182/blood.2020005588.
9. Tahir, S.K., Smith, M.L., Hessler, P., Rapp, L.R., Idler, K.B., Park, C.H., Leverson, J.D., and Lam, L.T. (2017). Potential mechanisms of resistance to venetoclax and strategies to circumvent it. BMC Cancer *17*, 399. https://doi.org/10.1186/s12885-017-3383-5.
10. Bose, P., Gandhi, V., and Konopleva, M. (2017). Pathways and mechanisms of venetoclax resistance. Leuk. Lymphoma *58*, 1–17. https://doi.org/10.1080/10428194.2017.1283032.
11. Kapoor, I., Bodo, J., Hill, B.T., Hsi, E.D., and Almasan, A. (2020). Targeting BCL-2 in B-cell malignancies and overcoming therapeutic resistance. Cell Death Dis. *11*, 941. https://doi.org/10.1038/s41419-020-03144-y.
12. Nechiporuk, T., Kurtz, S.E., Nikolova, O., Liu, T., Jones, C.L., D'Alessandro, A., Culp-Hill, R., d'Almeida, A., Joshi, S.K., Rosenberg, M., et al. (2019). The TP53 Apoptotic Network Is a Primary Mediator of Resistance to BCL2 Inhibition in AML Cells. Cancer Discov. *9*, 910–925. https://doi.org/10.1158/2159-8290.CD-19-0125.
13. Guieze, R., Liu, V.M., Rosebrock, D., Jourdain, A.A., Hernandez-Sanchez, M., Martinez Zurita, A., Sun, J., Ten Hacken, E., Baranowski, K., Thompson, P.A., et al. (2019). Mitochondrial Reprogramming Underlies

Resistance to BCL-2 Inhibition in Lymphoid Malignancies. Cancer Cell *36*, 369–384. https://doi.org/10.1016/j.ccell.2019.08.005.

14. Gorgun, G., Calabrese, E., Hideshima, T., Ecsedy, J., Perrone, G., Mani, M., Ikeda, H., Bianchi, G., Hu, Y., Cirstea, D., et al. (2010). A novel Aurora-A kinase inhibitor MLN8237 induces cytotoxicity and cell-cycle arrest in multiple myeloma. Blood *115*, 5202–5213. https://doi.org/10.1182/blood-2009-12-259523.
15. Kumari, G., Ulrich, T., Krause, M., Finkernagel, F., and Gaubatz, S. (2014). Induction of p21CIP1 protein and cell cycle arrest after inhibition of Aurora B kinase is attributed to aneuploidy and reactive oxygen species. J. Biol. Chem. *289*, 16072–16084. https://doi.org/10.1074/jbc.M114.555060.
16. Pham, L.V., Huang, S., Zhang, H., Zhang, J., Bell, T., Zhou, S., Pogue, E., Ding, Z., Lam, L., Westin, J., et al. (2018). Strategic Therapeutic Targeting to Overcome Venetoclax Resistance in Aggressive B-cell Lymphomas. Clin. Cancer Res. *24*, 3967–3980. https://doi.org/10.1158/1078-0432.CCR-17-3004.
17. Drakos, E., Singh, R.R., Rassidakis, G.Z., Schlette, E., Li, J., Claret, F.X., Ford, R.J., Jr., Vega, F., and Medeiros, L.J. (2011). Activation of the p53 pathway by the MDM2 inhibitor nutlin-3a overcomes BCL2 overexpression in a preclinical model of diffuse large B-cell lymphoma associated with t(14;18)(q32;q21). Leukemia *25*, 856–867. https://doi.org/10.1038/leu.2011.28.
18. Pan, R., Ruvolo, V., Mu, H., Leverson, J.D., Nichols, G., Reed, J.C., Konopleva, M., and Andreeff, M. (2017). Synthetic Lethality of Combined Bcl-2 Inhibition and p53 Activation in AML: Mechanisms and Superior Antileukemic Efficacy. Cancer Cell *32*, 748–760. https://doi.org/10.1016/j.ccell.2017.11.003.
19. Katayama, H., Sasai, K., Kawai, H., Yuan, Z.M., Bondaruk, J., Suzuki, F., Fujii, S., Arlinghaus, R.B., Czerniak, B.A., and Sen, S. (2004). Phosphorylation by aurora kinase A induces Mdm2-mediated destabilization and inhibition of p53. Nat. Genet. *36*, 55–62. https://doi.org/10.1038/ng1279.
20. Gully, C.P., Velazquez-Torres, G., Shin, J.H., Fuentes-Mattei, E., Wang, E., Carlock, C., Chen, J., Rothenberg, D., Adams, H.P., Choi, H.H., et al. (2012). Aurora B kinase phosphorylates and instigates degradation of p53. Proc. Natl. Acad. Sci. USA *109*, E1513–E1522. https://doi.org/10.1073/pnas.1110287109.
21. Diepstraten, S.T., Chang, C., Tai, L., Gong, J.N., Lan, P., Dowell, A.C., Taylor, G.S., Strasser, A., and Kelly, G.L. (2020). BCL-W is dispensable for the sustained survival of select Burkitt lymphoma and diffuse large B-cell lymphoma cell lines. Blood Adv. *4*, 356–366. https://doi.org/10.1182/bloodadvances.2019000541.
22. Di Veroli, G.Y., Fornari, C., Wang, D., Mollard, S., Bramhall, J.L., Richards, F.M., and Jodrell, D.I. (2016). Combenefit: an interactive platform for the analysis and visualization of drug combinations. Bioinformatics *32*, 2866–2868. https://doi.org/10.1093/bioinformatics/btw230.
23. Haddad, T.C., Suman, V.J., D'Assoro, A.B., Carter, J.M., Giridhar, K.V., McMenomy, B.P., Santo, K., Mayer, E.L., Karuturi, M.S., Morikawa, A., et al. (2023). Evaluation of Alisertib Alone or Combined With Fulvestrant in Patients With Endocrine-Resistant Advanced Breast Cancer: The Phase 2 TBCRC041 Randomized Clinical Trial. JAMA Oncol. *9*, 815–824. https://doi.org/10.1001/jamaoncol.2022.7949.
24. O'Connor, O.A., Özcan, M., Jacobsen, E.D., Roncero, J.M., Trotman, J., Demeter, J., Masszi, T., Pereira, J., Ramchandren, R., Beaven, A., et al. (2019). Randomized Phase III Study of Alisertib or Investigator's Choice (Selected Single Agent) in Patients With Relapsed or Refractory Peripheral T-Cell Lymphoma. J. Clin. Oncol. *37*, 613–623. https://doi.org/10.1200/JCO.18.00899.
25. Owonikoko, T.K., Niu, H., Nackaerts, K., Csoszi, T., Ostoros, G., Mark, Z., Baik, C., Joy, A.A., Chouaid, C., Jaime, J.C., et al. (2020). Randomized Phase II Study of Paclitaxel plus Alisertib versus Paclitaxel plus Placebo as Second-Line Therapy for SCLC: Primary and Correlative Biomarker Analyses. J. Thorac. Oncol. *15*, 274–287. https://doi.org/10.1016/j.jtho.2019.10.013.
26. Wolff, S., Erster, S., Palacios, G., and Moll, U.M. (2008). p53's mitochondrial translocation and MOMP action is independent of Puma and Bax and severely disrupts mitochondrial membrane integrity. Cell Res. *18*, 733–744. https://doi.org/10.1038/cr.2008.62.
27. Nieminen, A.I., Eskelinen, V.M., Haikala, H.M., Tervonen, T.A., Yan, Y., Partanen, J.I., and Klefström, J. (2013). Myc-induced AMPK-phospho p53 pathway activates Bak to sensitize mitochondrial apoptosis. Proc. Natl. Acad. Sci. USA *110*, E1839–E1848. https://doi.org/10.1073/pnas.1208530110.
28. Hoar, K., Chakravarty, A., Rabino, C., Wysong, D., Bowman, D., Roy, N., and Ecsedy, J.A. (2007). MLN8054, a small-molecule inhibitor of Aurora A, causes spindle pole and chromosome congression defects leading to aneuploidy. Mol. Cell Biol. *27*, 4513–4525. https://doi.org/10.1128/MCB.02364-06.
29. Manfredi, M.G., Ecsedy, J.A., Chakravarty, A., Silverman, L., Zhang, M., Hoar, K.M., Stroud, S.G., Chen, W., Shinde, V., Huck, J.J., et al. (2011). Characterization of Alisertib (MLN8237), an investigational small-molecule inhibitor of aurora A kinase using novel in vivo pharmacodynamic assays. Clin. Cancer Res. *17*, 7614–7624. https://doi.org/10.1158/1078-0432.CCR-11-1536.
30. Kojima, K., Konopleva, M., Samudio, I.J., Schober, W.D., Bornmann, W.G., and Andreeff, M. (2006). Concomitant inhibition of MDM2 and Bcl-2 protein function synergistically induce mitochondrial apoptosis in AML. Cell Cycle *5*, 2778–2786. https://doi.org/10.4161/cc.5.23.3520.
31. Ding, Y.H., Zhou, Z.W., Ha, C.F., Zhang, X.Y., Pan, S.T., He, Z.X., Edelman, J.L., Wang, D., Yang, Y.X., Zhang, X., et al. (2015). Alisertib, an Aurora kinase A inhibitor, induces apoptosis and autophagy but inhibits epithelial to mesenchymal transition in human epithelial ovarian cancer cells. Drug Des. Devel. Ther. *9*, 425–464. https://doi.org/10.2147/DDDT.S74062.
32. Blombery, P. (2020). Mechanisms of intrinsic and acquired resistance to venetoclax in B-cell lymphoproliferative disease. Leuk. Lymphoma *61*, 257–262. https://doi.org/10.1080/10428194.2019.1660974.
33. Haselager, M.V., Kielbassa, K., Ter Burg, J., Bax, D.J.C., Fernandes, S.M., Borst, J., Tam, C., Forconi, F., Chiodin, G., Brown, J.R., et al. (2020). Changes in Bcl-2 members after ibrutinib or venetoclax uncover functional hierarchy in determining resistance to venetoclax in CLL. Blood *136*, 2918–2926. https://doi.org/10.1182/blood.2019004326.
34. Seiller, C., Maiga, S., Touzeau, C., Bellanger, C., Kervoëlen, C., Descamps, G., Maillet, L., Moreau, P., Pellat-Deceunynck, C., Gomez-Bougie, P., and Amiot, M. (2020). Dual targeting of BCL2 and MCL1 rescues myeloma cells resistant to BCL2 and MCL1 inhibitors associated with the formation of BAX/BAK hetero-complexes. Cell Death Dis. *11*, 316. https://doi.org/10.1038/s41419-020-2505-1.
35. Blombery, P., Anderson, M.A., Gong, J.N., Thijssen, R., Birkinshaw, R.W., Thompson, E.R., Teh, C.E., Nguyen, T., Xu, Z., Flensburg, C., et al. (2019). Acquisition of the Recurrent Gly101Val Mutation in BCL2 Confers Resistance to Venetoclax in Patients with Progressive Chronic Lymphocytic Leukemia. Cancer Discov. *9*, 342–353. https://doi.org/10.1158/2159-8290.CD-18-1119.
36. Tausch, E., Close, W., Dolnik, A., Bloehdorn, J., Chyla, B., Bullinger, L., Döhner, H., Mertens, D., and Stilgenbauer, S. (2019). Venetoclax resistance and acquired BCL2 mutations in chronic lymphocytic leukemia. Haematologica *104*, e434–e437. https://doi.org/10.3324/haematol.2019.222588.
37. Blombery, P., Thompson, E.R., Nguyen, T., Birkinshaw, R.W., Gong, J.N., Chen, X., McBean, M., Thijssen, R., Conway, T., Anderson, M.A., et al. (2020). Multiple BCL2 mutations cooccurring with Gly101Val emerge in chronic lymphocytic leukemia progression on venetoclax. Blood *135*, 773–777. https://doi.org/10.1182/blood.2019004205.
38. Thijssen, R., Diepstraten, S.T., Moujalled, D., Chew, E., Flensburg, C., Shi, M.X., Dengler, M.A., Litalien, V., MacRaild, S., Chen, M., et al. (2021). Intact TP-53 function is essential for sustaining durable responses to

BH3-mimetic drugs in leukemias. Blood *137*, 2721–2735. https://doi.org/10.1182/blood.2020010167.

39. DiNardo, C.D., Tiong, I.S., Quaglieri, A., MacRaild, S., Loghavi, S., Brown, F.C., Thijssen, R., Pomilio, G., Ivey, A., Salmon, J.M., et al. (2020). Molecular patterns of response and treatment failure after frontline venetoclax combinations in older patients with AML. Blood *135*, 791–803. https://doi.org/10.1182/blood.2019003988.
40. Xu-Monette, Z.Y., Medeiros, L.J., Li, Y., Orlowski, R.Z., Andreeff, M., Bueso-Ramos, C.E., Greiner, T.C., McDonnell, T.J., and Young, K.H. (2012). Dysfunction of the TP53 tumor suppressor gene in lymphoid malignancies. Blood *119*, 3668–3683. https://doi.org/10.1182/blood-2011-11-366062.
41. Chen, X., Ko, L.J., Jayaraman, L., and Prives, C. (1996). p53 levels, functional domains, and DNA damage determine the extent of the apoptotic response of tumor cells. Genes Dev. *10*, 2438–2451. https://doi.org/10.1101/gad.10.19.2438.
42. Kracikova, M., Akiri, G., George, A., Sachidanandam, R., and Aaronson, S. A. (2013). A threshold mechanism mediates p53 cell fate decision between growth arrest and apoptosis. Cell Death Differ. *20*, 576–588. https://doi.org/10.1038/cdd.2012.155.
43. Fischer, M. (2017). Census and evaluation of p53 target genes. Oncogene *36*, 3943–3956. https://doi.org/10.1038/onc.2016.502.
44. Vousden, K.H., and Prives, C. (2009). Blinded by the Light: The Growing Complexity of p53. Cell *137*, 413–431. https://doi.org/10.1016/j.cell.2009.04.037.
45. Glover, D.M., Leibowitz, M.H., McLean, D.A., and Parry, H. (1995). Mutations in aurora prevent centrosome separation leading to the formation of monopolar spindles. Cell *81*, 95–105. https://doi.org/10.1016/0092-8674(95)90374-7.
46. Bischoff, J.R., and Plowman, G.D. (1999). The Aurora/Ipl1p kinase family: regulators of chromosome segregation and cytokinesis. Trends Cell Biol. *9*, 454–459. https://doi.org/10.1016/s0962-8924(99)01658-x.
47. Wysong, D.R., Chakravarty, A., Hoar, K., and Ecsedy, J.A. (2009). The inhibition of Aurora A abrogates the mitotic delay induced by microtubule perturbing agents. Cell Cycle *8*, 876–888. https://doi.org/10.4161/cc.8.6.7897.
48. Ryu, J., Pyo, J., Lee, C.W., and Kim, J.E. (2018). An Aurora kinase inhibitor, AMG900, inhibits glioblastoma cell proliferation by disrupting mitotic progression. Cancer Med. *7*, 5589–5603. https://doi.org/10.1002/cam4.1771.
49. Tomita, M., and Mori, N. (2010). Aurora A selective inhibitor MLN8237 suppresses the growth and survival of HTLV-1-infected T-cells in vitro. Cancer Sci. *101*, 1204–1211. https://doi.org/10.1111/j.1349-7006.2010.01499.x.
50. Nair, J.S., and Schwartz, G.K. (2016). MLN-8237: A dual inhibitor of aurora A and B in soft tissue sarcomas. Oncotarget *7*, 12893–12903. https://doi.org/10.18632/oncotarget.7335.
51. Liu, Q., Kaneko, S., Yang, L., Feldman, R.I., Nicosia, S.V., Chen, J., and Cheng, J.Q. (2004). Aurora-A abrogation of p53 DNA binding and transactivation activity by phosphorylation of serine 215. J. Biol. Chem. *279*, 52175–52182. https://doi.org/10.1074/jbc.M406802200.
52. Sasai, K., Treekitkarnmongkol, W., Kai, K., Katayama, H., and Sen, S. (2016). Functional Significance of Aurora Kinases-p53 Protein Family Interactions in Cancer. Front. Oncol. *6*, 247. https://doi.org/10.3389/fonc.2016.00247.
53. Kong, L.Z., Jia, X.H., Song, Z., Qiu, L.H., Li, L.F., Qian, Z.Z., Zhou, S.Y., Liu, X.M., Ren, X.B., Meng, B., et al. (2017). Co-targeting Aurora kinase A and Bcl-2 synergistically inhibits the viability in double-hit lymphoma cells. Transl. Cancer Res. *6*, 746–754. https://doi.org/10.21037/tcr.2017.06.41.

STAR★METHODS

KEY RESOURCES TABLE

REAGENT or RESOURCE	SOURCE	IDENTIFIER
Antibodies		
c-Myc (9E10)	Bio-Rad	Cat # MCA2200GA, RRID:AB_566935
Bcl2 (100)	Santa Cruz Biotechnology	Cat # sc-509, RRID:AB_626733
p-Bcl2 (ser70) (5H2)	Cell Signaling	Cat # 2827S, RRID:AB_659950
BCLxL (54H6)	Cell Signaling	Cat # 2764S, RRID:AB_2228008
Rabbit polyclonal Mcl1	ThermoFisher Scientific	Cat # PA5-86174, RRID:AB_2802967
Mcl1 (B-6)	Santa Cruz Biotechnology	Cat # sc-74436, RRID:AB_1126069
Rabbit polyclonal BAX	Cell Signaling	Cat # 2772S, RRID:AB_10695870
BAX (6A7)	Santa Cruz Biotechnology	Cat # sc-23959, RRID:AB_626728
BAK (D4E4)	Cell Signaling	Cat # 12105S, RRID:AB_2716685
Rabbit polyclonal PUMA	Cell Signaling	Cat # 4976S, RRID:AB_2064551
BIM (C34C5)	Cell Signaling	Cat # 2933S, RRID:AB_1030947
P53 (DO-1)	Santa Cruz Biotechnology	Cat # sc-126, RRID:AB_1030947
P21 Waf1/Cip1 (12D1)	Cell Signaling	Cat # 2947S, RRID:AB_823586
Mdm2 (SMP14)	Santa Cruz Biotechnology	Cat # sc-965, RRID:AB_627920
Rabbit polyclonal Caspase3	Cell Signaling	Cat # 9662S, RRID:AB_331439
Cdc42 (B-8)	Santa Cruz Biotechnology	Cat # sc-8401, RRID:AB_627233
Aurora A (D3E4Q)	Cell Signaling	Cat# 14475, RRID:AB_2665504
Phospho-Aurora A (Thr288)/Aurora B (Thr232)/Aurora C (Thr198) (D13A11)	Cell Signaling	Cat# 2914, RRID:AB_2061631
β-Actin (ACTBD11B7)	Santa Cruz Biotechnology	Cat # sc-81178, RRID:AB_2223230
m-IgGκ BP-HRP Antibody	Santa Cruz Biotechnology	Cat# sc-516102, RRID:AB_2687626
Goat polyclonal Secondary Antibody to Rabbit IgG - H&L (HRP)	Abcam	Cat# ab97051, RRID:AB_10679369
Vybrant DyeCycle Violet Stain	ThermoFisher Scientific	Cat #V35003
7AAD	BD Biosciences	Cat # 559925 RRID:AB_2869266
APC Annexin V	BioLegend	Cat # 640941
PE anti-human CD20	BioLegend	Cat # 302346 RRID:AB_2564144
FITC anti-human CD45	BioLegend	Cat # 304006 RRID:AB_314394
PE/Dazzle 594 anti-mouse CD45	BioLegend	Cat # 103146 RRID:AB_2564003
BID	Cell Signaling	Cat # 2022S RRID: AB_10692485
Bacterial and virus strains		
Lentivirus containing pLV[Exp]-U6>hTP53[shRNA#1]-U6>hTP53[shRNA#2]-U6>hTP53[shRNA#3]-CMV>EGFP:T2A:Puro	Vector Builder	Cat # LVS(VB201101-1148emb)-C (VB201101-1148emb)
Lentivirus containing pLV[Exp]-U6>Scramble_ shRNA#1-CMV>EGFP:T2A:Puro	Vector Builder	Cat # LVS(VB201101-1155xds)-C (VB201101-1155xds)
Chemicals, peptides, and recombinant proteins		
ABT199 (Venetoclax)	Selleck Chemicals	Cat #S8048
MLN8237 (Alisertib)	Selleck Chemicals	Cat #S1133

(*Continued on next page*)

Continued

REAGENT or RESOURCE	SOURCE	IDENTIFIER
AZD1152-HQPA/AZD2811 (Barasertib)	Selleck Chemicals	Cat #S1147
LY3295668 (AK-01)	Selleck Chemicals	Cat #S8782
Puromycin	Millipore Sigma	Cat #P8833-25MG
Qiazol Lysis Reagent	Qiagen	Cat # 79306
RG-7388 (Idasanutlin)	Selleck Chemicals	Cat #S7205
ABT199 (Venetoclax)	MedChemExpress	Cat # HY-15531
MLN8237 (Alisertib)	MedChemExpress	Cat # HY-10971
S63845	Selleck Chemicals	Cat #S8383
Cycloheximide solution, 100 mg/mL in DMSO, 0.2micron filtered	ThermoFisher Scientific	Cat # AAJ66004XF
FuGENE HD Transfection Reagent	Promega	Cat #E2311
Z-VAD-FMK	R&D Systems	Cat # FMK001
ReBlot Plus Strong Antibody Stripping Solution, 10x	Millipore Sigma	Cat # 2504
Critical commercial assays		
Pierce BCA Protein Assay Kit	ThermoFisher Scientific	Cat # 23227
CellTiter-Glo Cell Viability Assay	Promega	Cat #G7571
CellTiter-Glo 2.0 Cell Viability Assay	Promega	Cat #G9242
Clarity ECL Substrate	Bio-Rad	Cat # 1705060
Clarity Max ECL Substrate	Bio-Rad	Cat # 1705062
Muse Annexin V Dead Cell Assay Kit	Millipore Sigma	Cat # MCH100105
Deposited data		
RNA-seq Data	GEO (Gene Expression Ombibus) Accession Viewer	GSE200410
Experimental models: Cell lines		
WSU-NHL	DSMZ	DSMZ No. ACC 58 **RRID:CVCL_1793**
DoHH2	DSMZ	DSMZ No. ACC 47 **RRID:CVCL_1179**
VAL	DSMZ	DSMZ No. ACC 586 **RRID:CVCL_1819**
Mino	DSMZ	DSMZ No. ACC 687 **RRID:CVCL_1872**
Raji	ATCC	ATCC No. CCL-86 **RRID:CVCL_0511**
Ramos	ATCC	ATCC No. CRL-1596 **RRID:CVCL_0597**
COS-7	ATCC	ATCC No. CRL-1651 **RRID:CVCL_0224**
SU-DHL-4	ATCC	ATCC No. CRL-2957 **RRID:CVCL_0539**
SU-DHL-6	ATCC	ATCC No. CRL-2959 **RRID:CVCL_2206**
Experimental models: Organisms/strains		
SCID mice (CB17/Icr-*Prkdc*^{scid}/IcrIcoCrl)	Charles River Laboratories	Strain Code 236
NCG mice (NOD-*Prkdc*^{em26Cd52}*Il2rg*^{em26Cd22}/NjuCrl)	Charles River Laboratories	Strain Code 572
BALB/c mice	Charles River Laboratories	Strain Code 028
Recombinant DNA		
NanoBRET PPI Control Pair (P53, Mdm2)	Promega	Cat #N1641

(*Continued on next page*)

Continued

REAGENT or RESOURCE	SOURCE	IDENTIFIER
Software and algorithms		
GraphPad Prism 9.0	GraphPad Software, Inc	GraphPad Prism, RRID:SCR_002798 https://www.graphpad.com/scientific-software/prism/
Kaluza Analysis 2.1	Beckman Coulter Life Sciences	Kaluza, RRID:SCR_016182 https://www.beckman.com/flow-cytometry/software/kaluza
Combenefit	Jodrell, Cancer Research UK	https://www.cruk.cam.ac.uk/research-groups/jodrell-group/combenefit
ImageJ	Wayne Rasband, NIH	ImageJ, RRID:SCR_003070 https://imagej.nih.gov/ij/download.html
Ingenuity Pathway Analysis	Qiagen	Ingenuity Pathway Analysis, RRID:SCR_008653 https://digitalinsights.qiagen.com/products-overview/discovery-insights-portfolio/analysis-and-visualization/qiagen-ipa/

EXPERIMENTAL MODEL AND SUBJECT DETAILS

Mice

All animal experiments were conducted under a protocol approved by the Institutional Animal Care and Use Committee (IACUC) of Atrium Health. 4–6 week old female CB17-SCID and NCG mice were purchased from the Charles River Laboratories (Wilmington, MA, USA).

Cell lines

DoHH-2 (DSMZ Cat# ACC-47, RRID:CVCL_1179), VAL (DSMZ Cat# ACC-586, RRID:CVCL_1819), WSU-NHL (DSMZ Cat# ACC-58, RRID:CVCL_1793), and Mino (DSMZ Cat# ACC-687, RRID:CVCL_1872) cell lines were purchased from DSMZ (Brunswick, DEU). The Burkitt lymphoma cell lines Raji (CLS Cat# 300359/p25072_RAJI, RRID:CVCL_0511) and Ramos (CLS Cat# 302007/p32087_Ramos, RRID:CVCL_0597) were purchased from ATCC (Manassas, VA, USA). Cells were cultured in RPMI1640 medium supplemented with 10% heat-inactivated FBS (R&D Systems, Minneapolis, MN, USA), 10,000 IU/mL penicillin-streptomycin (Fisher Scientific, Waltham, MA, USA), and 200mM L-glutamine (Fisher Scientific) at 37°C and 5% CO2.

METHOD DETAILS

Cytotoxicity assays

Cells in the exponential growth phase were plated at 3×10^5 cells/mL in 96-well plates and treated with venetoclax (40 nM), MLN8237 (50 nM), a combination of the two, or dimethyl sulfoxide (DMSO) vehicle, as indicated by the figures and corresponding figure legends, for 24, 48, or 96-h timepoints. Cell viability was assessed by ATP quantification using CellTiter-Glo assays (Promega, Madison, WI, USA) according to the manufacturer's instructions and was read on a SpectroMax plate reader. Additional cytotoxicity and apoptosis assays were performed using the Muse Annexin V & Dead Cell Kit (EMD Millipore, Burlington, MA, USA) following the manufacturer's protocol, and analyzed using a Guava Muse Cell Analyzer (EMD Millipore).

Cell cycle and apoptosis assay

Concurrent cell cycle and apoptosis assays were performed using Vybrant Dyecycle Violet stain and annexin-V (ThermoFisher Scientific, Waltham, MA, USA) and analyzed using flow cytometry. Briefly, 1 x 10^6 cells were collected after 24–48 h of indicated treatment and washed once via centrifugation (300g, 5 min) with HBSS. Supernatants were carefully decanted without disturbing the cell pellet. Cells were then resuspended in 1mL of PBS with 1X annexin binding buffer and 1 μL of Dyecycle stain plus 5 μL of 7AAD (BD Biosciences Cat# 559925, RRID:AB_2869266) and 5 μL of annexinV-AF488 (BD Biosciences, San Jose, CA, USA). Cells were then placed in an incubator at 37°C for 30 min before analysis on a LSRFortessa flow cytometer (BD Biosciences) at LCI Immune Monitoring Core. Flow cytometric data were analyzed using Kaluza software (Kaluza, RRID:SCR_016182).

Immunoblotting

Cell lysates were prepared using RIPA Lysis and extraction buffer (Thermo Fisher Scientific) supplemented with 1x phosphatase and protease inhibitor tablets (Sigma-Aldrich, St. Louis, MO, USA) at a density of 1×10^6 cells/100 μL. Cell lysates were quantified using BCA assays (Thermo Fisher Scientific), and equal amounts of denatured protein samples were loaded onto 4–20% SDS-PAGE gels (Bio-Rad, Hercules, CA, USA) for electrophoresis. After electrophoresis, the proteins were transferred to nitrocellulose membranes,

blocked in 5% non-fat milk for 1 h, and incubated overnight at 4°C with the indicated primary antibody (dilution as recommended by manufacturers) in 5% non-fat milk. The following day, the membranes were washed 4x for a total of 30 min and then incubated with HRP-labeled secondary antibodies for 2 h at room temperature. After another four washes, signals were developed using Clarity Western ECL substrate or Clarity Max Western ECL substrate (Bio-Rad). Images were captured using a UVP GelDoc-It Imaging System and accompanying software to scan the immunoblots (Analytik Jena, Jena, DEU). To re-probe a membrane, immunoblots were incubated with 1x ReBlot Stripping Solution (Millipore Sigma) for 30 s, followed by 3 washes for 5 min each. Membranes were then blocked in 5% milk for 30 min and incubated with antibodies as described. Determination of band intensity was performed using ImageJ software (ImageJ, RRID:SCR_003070).

NanoBRET Bioluminescence Resonance Energy Transfer (BRET) assay

2×10^6 COS-7 cells were transfected in T75 flasks using FuGENE HD Transfection Reagent with 5 μg p53 HaloTag Fusion Vector and 1 μg of NanoLuc-Mdm2 Fusion Vector (PROMEGA catalog N1614) for ~24 h at 37°C and 5% CO2. The cells were washed once with PBS and tyrpsinized in 2 mL of 0.05% trypsin-EDTA. 2 mL of cell culture media was used to neutralize trypsin, and the cells were spun at 125xg for 5 min. Cells were resuspended at 2×10^5 cells/mL in Opti-MEM Reduced Serum Media, no phenol red, and 4% FBS. Cells were aliquoted for treatment with vehicle, venetoclax, MLN8237, or their combination. Treated cells were then divided into two pools, so that each sample set would receive either 100 nM 618 ligand or DMSO. Cells were seeded in white-walled 96-well plates in triplicate with 100 μl per well and incubated for ~24 h at 37°C and 5% CO2. NanoBRET Nano-Glo Substrate was prepared following the manufacturer's instructions, and the plates were read for donor emission (460nm) and acceptor emissions (618 nm) on a SpectroMax plate reader.

Real-time PCR and mRNA quantification

Cells were pelleted after the indicated treatments, washed once with PBS, lysed in TRIzol buffer, and stored at −80°C until further processing at the LCI Molecular Biology Core. Total RNA was isolated using the miRNeasy Mini Kit (Qiagen). RNA concentration was determined using the Qubit High Sensitivity RNA HS assay kit (Thermo Fisher Scientific, Waltham, MA, USA). RNA integrity was verified using an Agilent 2100 Bioanalyzer (Agilent Technologies, Santa Clara, CA, USA). First-strand complementary DNA was synthesized using an iScript cDNA synthesis kit (Bio-Rad, Hercules, CA, USA). The reverse transcription reaction was performed on an ABI ProFlex PCR System (Applied Biosystems, Foster City, CA, USA) at 42°C for 30 min and stopped by heating to 85°C for 5 min. Fifty nanograms of the final product was used as a template for PCR. qRT-PCR was performed using TaqMan Probe-Based Detection (Applied Biosystems) according to the manufacturer's instructions on an ABI 7500 Fast Real-Time PCR System. Taqman gene expression assays were used (*BCL2*: Hs00608023_m1, *MYC*: Hs00153408_m1, BAX: Hs00180269_m1, BAK: Hs00832876_g1, TP53: Hs01034249_m1, Applied Biosystems) together with Taqman Gene Expression Master Mix (Applied Biosystems). The template was amplified by 40 cycles of denaturation at 95°C for 15 s, annealing of primers and probe, and extension at 60°C for 1 min in triplicates. Fluorescence data were acquired during the combined annealing/extension step. RT-negative reactions were performed on each plate to confirm the absence of DNA contamination. Fold changes in mRNA were quantified by the comparative Ct method after normalization to β-actin (ACTB: Hs01060665_g1) internal control and vehicle (drug) control using the 2ΔΔCT method.

Murine xenograft studies

Subcutaneous (SC) lymphoma xenografts were established by injecting 1×10^6 DoHH2 cells into the right flank of anesthetized SCID mice. Animals were randomized 14–28 days after inoculation, when tumor sizes reached 10–15 mm in diameter. Disseminated models were produced by injecting 2×10^5 VAL cells into the lateral tail vein of NCG mice, and the animals were randomized into the treatment groups 5 days after injection. For both models, mice were randomized into four different treatment groups (vehicle, MLN8237, venetoclax, and VEN+MLN8237) of 6–8 mice per group. Treatment doses were administered to mice as MLN8237 (40 mg/kg/d via oral gavage), venetoclax (50 mg/kg/d via oral gavage), or a combination of both MLN8237 and venetoclax. The control group received the vehicle formulation (5% DMSO, 50% PEG 300, 5% Tween80 + 40%ddH2O via oral gavage). Treatments were performed five days a week for three weeks. Mice were monitored for an additional 80-day for response and survival evaluation. In one sub-study, SC xenograft tumors were excised after three days of treatment for RNA sequencing. Animals were monitored daily for tumor volume, and body weight was measured twice weekly. Mice were euthanized if the xenografts exceeded 10% of their total body weight, caused clear discomfort or impaired ambulation, or if a mouse lost more than 20% of its baseline body weight. Some non-grafted NCG animals (3/group) were administered the indicated drugs to evaluate toxicity. After three weeks of treatment, blood, serum, and vital organs were harvested and evaluated for toxicity. Serum biochemistry analysis and H&E staining of 10% formalin-fixed tissues were performed at the IDEXX laboratory (Westbrook, ME, USA). Anti-human CD45 (HI30) (BioLegend Cat# 304006, RRID:AB_314394), anti-human CD20 (2H7) (BioLegend Cat# 302346, RRID:AB_2564144), and anti-mouse CD45 (30-F11) (BioLegend Cat# 103146, RRID:AB_2564003) antibodies (BioLegend, San Diego, CA) were used to evaluate disseminated tumors in xenografted mouse tissues by flow cytometry. The IACUC approved protocol for this study specified the tumor burden humane endpoint as any tumor measuring greater than 2 cm at the largest diameter. (IACUC approved protocol #02-18-02A titled "Combined Inhibition of Signaling Pathways for Treatment of Non-Hodgkin Lymphoma").

Next generation sequencing and quantification of mRNA in tumor grafts

Transcriptome profiling was performed using RNA sequencing of excised tumors in the Molecular Biology Core Laboratory at the LCI. Sequence alignment and curation were performed by bioinformaticians at the Center for Biostatistics at the LCI. Briefly, excised tumor tissues were snap-frozen until total RNA was isolated using the miRNeasy Mini Kit (Qiagen) according to the manufacturer's instructions. RNA integrity was evaluated using an Agilent 2100 Bioanalyzer (Agilent Technologies). Ribosomal RNA was selectively depleted using RiboZero Globin (Illumina, San Diego, CA). Next-generation sequencing libraries were prepared using an Illumina TruSeq Stranded Total RNA kit (Illumina). RNA was fragmented using divalent cations at elevated temperatures, following purification. The cleaved RNA fragments were copied into first-strand cDNA using reverse transcriptase and random primers. Strand specificity was achieved by replacing dTTP with dUTP during the second-strand cDNA synthesis. The products were amplified using PCR and purified to create the final cDNA library. The libraries were sequenced on an Illumina NextSeq 500 using High-Output Kits v2.5 (150 cycles).

RNA sequence files in fastq format were transferred from the Illumina BaseSpace Hub to the SevenBridges platform for sequence alignment with human (GRh38) and murine (mm10) reference genomes using STAR aligner for deduplication and to exclude sequences of murine origin amplified due to contamination from xenograft harvest. Paired-end reads that exclusively fit the human references were processed for further analysis. Significantly expressed genes were clustered across treatment groups in an unsupervised manner and further used in Ingenuity pathway analysis (IPA) (Ingenuity Pathway Analysis, RRID:SCR_008653) to identify networks of importance and other interactions relevant to the disease and treatment.

Creation of p53 knockdown cell lines using lentivirus

Lentiviral vectors containing scrambled or TP53 shRNA were packaged into viral particles by VectorBuilder (Guangzhou, China). Viral particles were used to infect DoHH2 cells in culture media at a multiplicity of infection (MOI) of 20–30. Immediately after the addition of viral particles, the cells were centrifuged at 1000 g for 1 h, and the supernatant was removed, and the cells resuspended in fresh culture medium. After 72 h, cultures were treated with the selection antibiotic puromycin (0.6 μg/ml) for 48–72 h period. Selected cells were expanded and used in subsequent experiments. Knockdown of the p53 protein was confirmed by immunoblotting.

Statistics

All *in vitro* experiments were performed with at least three technical or experimental replicates unless otherwise specified. GraphPad Prism (GraphPad Prism, RRID:SCR_002798) was used to fit the nonlinear regression for dose-response curves. The log rank test was used to analyze survival data from xenograft experiments. Synergy/antagonism analyses were performed using Cancer Research UK Cambridge Institute's Combenefit (Cambridge, UK).

QUANTIFICATION AND STATISTICAL ANALYSIS

Statistics were performed using Graph Pad Prism 10 Software. Tests included multiple unpaired t-test, one-way ANOVA with multiple comparisons, and survival curve comparison with log rank (Mantel-Cox) test. Densitometry values from western blots were measured vis ImageJ software. Tests used and significance metrics, such as statistical tests used, the exact value of n, definition of center, and dispersion and precision measured, are described in figure legends. Significance is shown in figures as $^{****}p < 0.0001$, $^{***}p < 0.001$, $^{**}p < 0.01$, $^{*}p < 0.05$, or ns (not significant).